Synergies of nanocopper and graphene as co-fillers in a shape-memory polyurethane

Jeet Vishwakarma[1,2], Shubham Jaiswal[1,2], Sarvesh Kumar Gupta[1], Nikhil Gorhe[1,2], Dipen Kumar Rajak[1], Prasanth N[1], Reuben J. Yeo[3], Chetna Dhand[1,2,*], Neeraj Dwivedi[1,2,*]

[1]CSIR-Advanced Materials and Processes Research Institute, Bhopal- 462026, India

[2]Academy of Scientific and Innovative Research (AcSIR), Ghaziabad- 201002, India

[3]Institute of Materials Research and Engineering (IMRE), Agency for Science, Technology, and Research (A*STAR), 2 Fusionopolis Way, Innovis #08-03, Singapore 138634, Singapore

*Corresponding Author

[*] **Email:** neeraj.dwivedi@ampri.res.in **and** neerajdwivedi6@gmail.com(N. Dwivedi)

chetna.dhand@ampri.res.in **and** chetnachem24@gmail.com(C. Dhand)

Abstract

Graphene and its related materials are commonly used as reinforcements in shape-memory-polymers (SMPs) to engineer their functional properties, but at the cost of a reduction in their failure strain. Here, we demonstrate that the reduced failure strain in multilayer graphene reinforced polyurethane (PU/MGR) composites (at 2.0 wt% MGR) could be enhanced by more than two times with the introduction of copper nanoparticle (CuNP) co-fillers (0.1–1.0 wt% CuNP). The CuNPs play a crucial role in disrupting the π-π and van der Waals interactions between the MGR sheets, which serve to reduce their agglomeration and suppress the number of stress concentration sites. Interestingly, introduction of CuNPs was found to not only increase the failure strain, but also contribute to remarkable tribological and thermal properties of the PU/MGR/CuNP composites. CuNP-decorated MGR fillers present at a sliding tribo-interface enabled the easy shearing and rolling of MGR sheets across each other, thereby significantly reducing the friction to attain a state of superlubricity exhibiting an ultralow and stable coefficient of friction of ~0.05–0.06. These concepts derived from using CuNPs as co-fillers in graphene-reinforced PU may be extended to many other SMP systems for various functional systems.

Keywords: Shape memory polymers, graphene fillers, nanoparticulate fillers, strain enhancement, tribology and thermal conductivity

Introduction

Since its discovery, graphene and its related materials have attracted huge attention due to their extraordinary physicochemical and functional properties [1]. Graphene has shown very high electron mobility [2], high electrical and thermal conductivities [3], and excellent mechanical and tribological characteristics [4]. These astonishing properties have also led to their exploration as fillers to engineer the characteristics of metals [5], ceramics [6], and polymers [7]. Furthermore, the application of graphene-based materials has led to improved thermal conduction [8] and electrical transport [9] in many polymers.

One of the long-standing issues in graphene research is that the reinforcement of polymeric systems using graphene-based materials drastically degrades the polymer composite's failure strain [10]. A significant reduction in the failure strain was observed in graphene-reinforced shape memory polymers (SMPs) [11], a category of intelligent polymers with shape memory effect that is a rising star for the next generation of biomedical devices, soft robotics, micro-/nano-electromechanical systems (MEMS/NEMS), actuators, and sensors. [12]. Jung et al. showed that the introduction of few-layer graphene enhanced the thermal conductivity of shape memory polyurethane (PU) but reduced its failure strain by 22% [13]. Sofla et al. found improved electrical conductivity but reduced failure strain for PU reinforced with graphene-based materials [14]. Abbasi et al. synthesized PU/graphene nanoplatelet composites and found improved electrical properties but reduced mechanical strain [15]. Shi et al. developed a shape memory PLA/natural rubber/tetrapod zinc oxide/graphene composite and found that while the introduction of 2.5 wt% of graphene increased the thermal conductivity, it significantly reduced the failure strain [16]. Jiu et al. performed in-situ synthesis of highly concentrated graphene cross-linked PU composites and found improved electrical conductivity but reduced failure strain [17]. However, researchers tried to solve this problem not specifically with PU and graphene, but with the other polymer and graphene related material. Polyamide's

failure strain decreases with graphene oxide (GO) but increases significantly with a GO-carbon nanotube hybrid[18]. In epoxy, GO reduces failure strain, while functionalized GO with poly(ethylene adipate) increases failure strain[19]. Poly(vinyl chloride) shows reduced failure strain with GO, which improves with glycerol addition through a drop in tensile strength occurred [20]. Polypropylene's strain at break decreases drastically with graphene nanoplatelets (GnP) but increases substantially in a PP/SEBS/GnP blend, with a reduction in tensile strength[21]. These investigations showed that graphene reinforcement is a critical drawback for polymeric materials from a mechanical failure strain viewpoint. Controlling the degradation of the mechanical failure strain of graphene-reinforced polymer composite systems therefore necessitates creative and effective strategies to be adopted without adversely affecting their functional properties including thermal conductivity, actuation, shape memory, and electrical conductivity, among others.

Low friction and high wear resistance are primary requirements in materials/components to develop energy-efficient and sustainable moving mechanical technologies. However, many soft polymeric materials are highly susceptible to wear and exhibit moderate-to-high friction when sliding against harder counterfaces [22]. For SMPs in particular, certain pre-programmed steps are required to ensure that the SMP deforms and recovers to the desired shape. Both deformation and shape recovery depend on the external environment and mechanical stimuli which can cause high friction and damage/scratches to the surface of SMP. Moreover, friction during shape recovery of SMP components on contacting surfaces can minimize shape recovery and even increase the energy required for actuation. Additionally, SMPs are also promising options for developing self-healable and sustainable nano-/micro-/macro-machines. Therefore, for maximum utilization of the SMP on contacting surfaces, low friction and high wear resistance are necessary.

In this work, we have adopted a unique approach of introducing multilayer graphene (MGR) dressed with copper nanoparticles (CuNP) as fillers to engineer shape memory PU, hereon denoted as MGR/CuNP binary fillers. The co-reinforcement of CuNP with MGR extraordinarily suppressed the elongation-reducing nature of MGR and largely increased the failure strain of the resultant PU/MGR/CuNP composite compared to PU/MGR composite. Interestingly, PU/MGR/CuNP yielded improved thermal conductivity, faster actuation, lower friction and higher wear resistance than the PU/MGR composite, suggesting that MGR/CuNP as a binary filler can drastically boost the performance of PU.

Experimental Section

Materials: PU granules (MM5520, ether type) with melt flow index of 3.1 g/10 min and extruding temperature range of 190 to 210 ℃ were used as the model SMP PU matrix procured from the *SMP technologies Japan*. Multilayer graphene (MGR) and copper nanoparticles (CuNP) were introduced as fillers to develop CuNP dressed MGR filler reinforced PU-composites procured from the *SRL, Inc*. The thickness of MGR flakes was around 11–15 nm.

Synthesis of PU composites: A twin screw micro-compounder (*Thermo Haake MiniLab 3*) attached with a mini-injection molding tool (*Thermo Scientific HAAKE MiniJet Pro Piston*) was used to manufacture PU composites of desired shapes and sizes, as illustrated in Figure 1. The PU granules were initially washed with ultrapure water and then dried in an oven to remove moisture. During sample processing, the twin screw speed and micro-compounder temperature were maintained at 60 rpm and 200°C, respectively. After blending for 15 minutes, the mixture was placed inside a cylinder heated to 205°C. Subsequently, the mixture was fed into the die using a piston at a pressure of 620 bar for 5 seconds, followed by maintaining a post pressure of 400 bar for 15 seconds. Pristine PU (sample S1) and PU/MGR composite containing 2 wt%

MGR filler (sample C0) were used as the reference samples. The subsequent series of samples were prepared by introducing and varying the wt% of the secondary CuNP filler to obtain concentrations of 0.1%, 0.25%, 0.5%, and 1% in the PU/MGR composite. The resultant PU/MGR/CuNP composite samples with 0.1%, 0.25%, 0.5%, and 1% wt% of CuNP are labelled as samples C1, C2, C3, and C4, respectively.

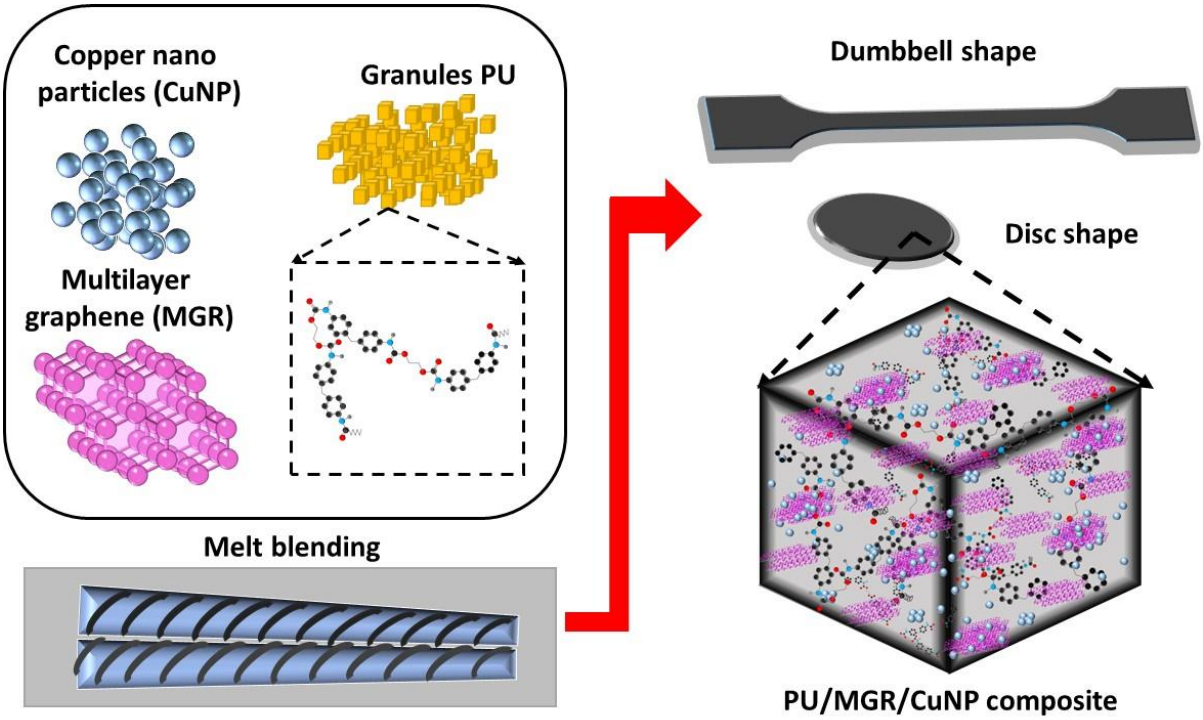

Figure 1: Schematic illustration showing the preparation of a PU/MGR/CuNP composite by the melt blending method using a twin-screw micro-compounder.

Characterizations of the materials and PU composites: The prepared samples were characterized using various spectroscopic and microscopic techniques such as Raman spectroscopy, X-ray diffraction (XRD), field-emission scanning electron microscopy (FESEM), and Fourier transform infrared (FTIR) spectroscopy. X-ray diffractometers (*Bruker D8 Advance (Germany) and Rigaku miniflex (Japan)*) with Cu K_α radiation (λ = 0.154 nm) were used to assess the crystallographic structures of the MGR and CuNP fillers, with measurements performed in 2θ angle range of 10^o to 70^o. The morphologies of the filler

materials and the PU composites were examined using FESEM (*NOVA Nanosem 430*). For FESEM analysis of the PU composites, cryo-fractured samples were prepared followed by the application of a conductive gold layer on the fractured surfaces to reduce surface charging during imaging. FTIR measurements (*Nicolet iS50, USA*) were performed within a wavenumber range of 4000 cm^{-1} to 400 cm^{-1} to probe the molecular structures, chemical bonding, and the presence of any functional groups in the pristine PU and PU composite samples. The thermal properties of pristine PU and PU composite samples were investigated using differential scanning calorimetry (*DSC, Mettler Toledo*) at a heating and cooling rate of 10 °C/min. Two cycles were performed and the heating curve of the 1st cycle was analysed. The thermal conductivities of the samples were measured using a laser flash method (*NETZSCH LFA467 Hyper Flash*). Uniaxial tensile tests (*Tinius and Olsen H25KT* universal testing machine) were performed on pristine PU and PU composite samples to estimate various mechanical parameters such as ultimate tensile stress, elongation at break, toughness and elastic modulus. The tensile tests were performed on dogbone samples prepared using melt blending and injection molding according to the ISO 527-2 standard. The repeatability of the results was checked on at least 8–10 samples. Friction and wear measurements were performed on PU and PU composite samples using a ball-on-disk low-load tribometer (*Ducom, India*) in rotary mode under controlled conditions (24 °C, RH 35±5%). A stainless-steel ball (hardened chrome steel ball grade 52100 from *Simply bearings, UK*) 2 mm in diameter was used as the counterface material. The tests were performed along a 2 mm diameter track at a speed of 100 rpm for 1 h, corresponding to 6000 frictional cycles. A constant normal load of 1 N was applied throughout the test, and at least three measurements were performed on each type of sample for repeatability of the results. After each test, images of the ball and the sample surface (where the test had been conducted) were captured using an optical microscope to observe the extent of wear.

Shape memory thermomechanical tests: Constrained shape recovery thermo-mechanical tests were performed in a computer-controlled *Tinius Olsen H25KT* universal testing machine equipped with a controlled environment chamber. A programmed cycle of heating, deformation, shape fixation, and recovery was carried out with a 1 kN load cell [23]. The shape fixity ratio (R_f) and shape recovery ratio (R_r) were calculated using Equations 1 and 2, respectively:

$$R_f = \frac{L_u - L_i}{L_s - L_i} \quad (1)$$

$$R_r = \frac{L_u - L_r}{L_u - L_i} \quad (2)$$

where L_s is the deformation length, L_u is the fixed length (length at temporary state), L_i is the initial length and L_r is the recovered length of the sample. Next, the shape memory tests were also performed in hot water environment to study in-depth the shape memory behavior of PU and the PU composite samples. The shape memory test comprised a four-step program of a) heating of the sample at 75 ℃ for 10 min, b) deformation of the sample to a 30° angle, c) cooling of the sample at 30 ℃ for 10 min, and d) exposure of the sample to 75 ℃ to check the shape recovery and shape recovery rate. The R_f and R_r values were calculated for these samples using Equations 3 and 4:

$$R_f = \frac{150^\circ - \theta_f}{150^\circ} \quad (3)$$

$$R_r = \frac{\theta_r}{150^\circ} \quad (4)$$

where θ_f is the angle for the fixed temporary shape after cooling the sample and θ_r is the angle of the recovered shape after heating the sample above its glass transition temperature, T_g.

Result and Discussion:

Prior to their incorporation into PU, the MGR and CuNP fillers used in this work were thoroughly characterized. The XRD pattern (Figure 2a) of MGR showed peaks at 26.3° and 54.6° corresponding to the characteristic crystallographic planes of (002) and (004), respectively, in graphitic carbon, as desired for MGR [24]. Likewise, the XRD pattern in Figure 2a exhibited the characteristic peaks of crystalline CuNP at 43.1° and 50.1° corresponding to the crystallographic planes of (111) and (200) in Cu, respectively [25]. Additionally, the peaks at 35.3° and 38.4° correspond to the crystallographic planes of (111) and (200), respectively of copper oxide [26], suggesting that some of the CuNPs were oxidized prior to sample preparation. FESEM images of the filler materials showed the layered structure of graphene for MGR (Figure 2b) and the existence of nanoscale CuNP particles and their clustering (Figure 2c), which were consistent with what was to be expected for these materials. Next, we discuss the characterization of pristine PU and PU composites containing MGR fillers and MGR/CuNP binary fillers. At first glance, the FTIR spectra of pristine PU and PU composites look fairly similar regardless of the type of filler (Figure 2d-e). The analysis revealed that the FTIR spectra of all the samples are dominated by the PU peaks, *i.e.* the peaks corresponding to CH, NH, CO, and CONH vibrations of PU are present in all the samples. Nonetheless, NH and CH bonding regions of the FTIR was enlarged for all the samples to further assess bonding changes between the samples, if any present (Figure 2e). The NH and CH bonding regions also looked similar for all the samples. From the FTIR spectra, it was concluded that the reinforcement of PU with either MGR or MGR/CuNP binary fillers did not adversely affect the characteristic bonding of PU (Figure 2d-e). This implies that the shape memory characteristic of PU would not be compromised. Further, the XRD patterns (Figure 2f) revealed the presence of all the characteristic peaks of MGR (such as the (002) and (004) crystallographic planes of MGR) and CuNP (111) and (200) crystallographic planes of Cu in MGR and MGR/CuNP reinforced PU-composites. In addition, all the samples including pristine PU showed a broad hump around 2θ

of 20° (Figure 2f) corresponding to the PU matrix [27]. DSC measurements were performed to study the thermal properties of pristine PU and PU composites, especially to quantify glass transition temperature (T_g) of mixed phase of PU. From DSC curves (Figure 2g), we found Tg of 56.0 in PU, which is in agreement with the reported literature for the same grade of PU[28]. The Tg remains similar in the PU/MGR composite which could be due to non-covalent interaction between the PU chains and MGR sheets. However, Tg slightly decreases to about 50.8-51.3 in PU/MGR/CuNP composite depending upon CuNP concentration. The decrease of Tg may be attributed to CuNP induced reduction of non-covalent interaction between PU chains and the MGR sheets.

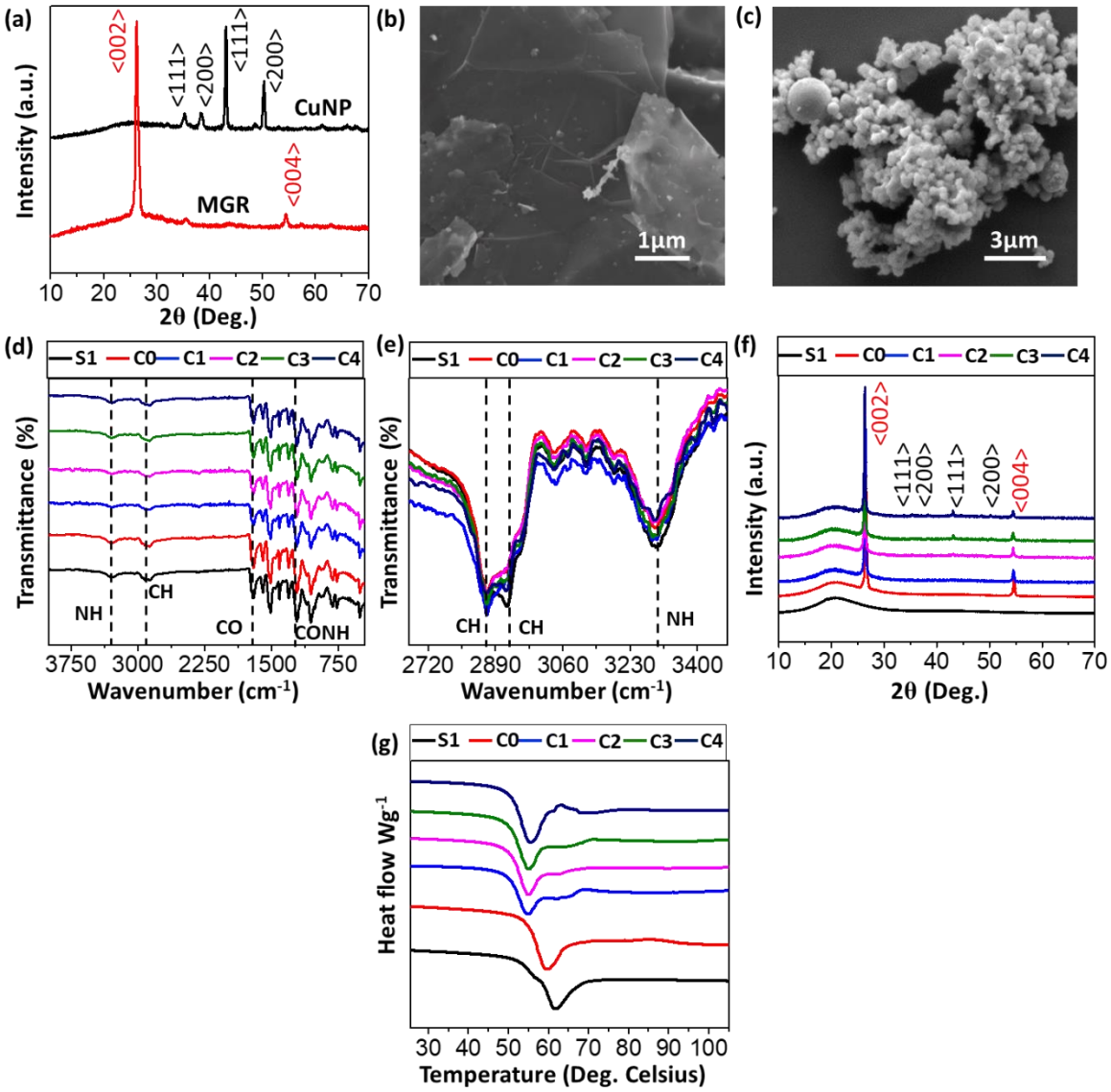

Figure 2: (a) XRD patterns of MGR and CuNP. FESEM images of (b) MGR and (c) CuNP. (d-e) FTIR, (f) XRD, and (g) DSC characterizations of pristine PU and PU-composites.

Table 1: Thermal properties of PU and PU composites.

Sample	Glass transition temperature T_g (°C)
S1	56.0
C0	55.8
C1	50.9
C2	50.9
C3	50.8
C4	51.3

Next, we focus on the tensile properties of the PU and PU composite samples by analyzing their stress-strain curves (Figure 3a). The curves exhibit distinct regions with increasing strain that represent the material's elastic behavior, yielding, and plastic deformation accompanied by cold drawing. After yielding, continuous deformation of the material causes necking along the gauge length. A typical ductile-like behavior was observed in pristine PU (sample S1) with an average failure strain of ~277% (Figure 3b). Strain hardening, a mechanism where the applied strain increases the tensile strength until fracture, was also noticed in these samples (Figure 3a). Importantly, the incorporation of MGR into PU (sample C0) was found to degrade the strain by limiting the average failure strain to just ~46% (Figure 3b). Such a huge reduction in the failure strain of PU due to MGR reinforcement is detrimental for practical applications of shape memory polymer composites. This prompted us to discover new approaches to recover (or enhance) the failure strain of PU/MGR as much as possible while maintaining or further improving the necessary thermal, actuation, and other mechanical characteristics of the MGR-reinforced PU composites.

We introduced CuNP in PU/MGR composites having a fixed MGR concentration of 2 wt%. The introduction of just 0.1 wt% of CuNP (sample C1) immensely increased the average failure strain from ~46% for the PU/MGR composite (sample C0) to 155% in the

PU/MGR/CuNP composite (sample C1) (Figure 3b). However, increasing the CuNP concentration from 0.1 wt% to 1.0 wt% (samples C1 to C4) did not further alter the failure strain as confirmed by a saturation in the trend, with average failure strains of ~147%, ~145% and ~146% in samples C2, C3, and C4, respectively (Figure 3b). Upon closer examination, we noticed that the relative improvement of the failure strain in the PU/MGR/CuNP composite was roughly three times that of PU/MGR composite (sample C0), i.e. an absolute change in the failure strain from ~46% for the PU/MGR composite (sample C0) to almost 150% and above for the PU/MGR/CuNP composite (samples C1 to C4). We further quantified the toughness of PU (sample S1) and its composites C0 to C4 and the trend was found to be similar to failure strain results, where the addition of CuNPs to MGR-reinforced PU improved the toughness, but reached a saturation in the extent of toughness enhancement with a further increase in CuNP concentration (Figure 3c). As the failure strain directly influences the toughness of the composite, the introduction of CuNP directly contributed to the enhanced toughness of the PU/MGR/CuNP composites. This implied that more energy was required to fracture the PU/MGR/CuNP composites compared to the PU/MGR composite.

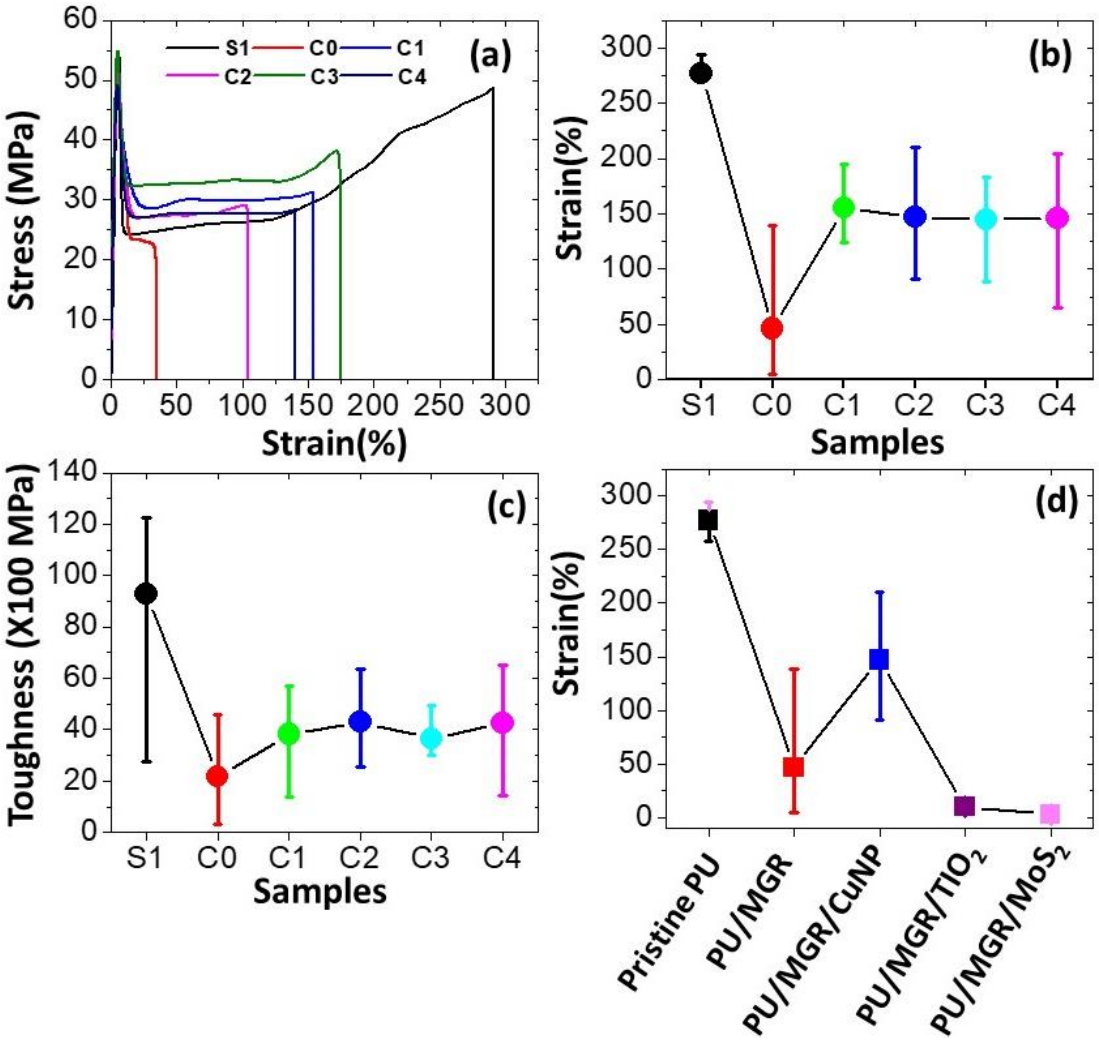

Figure 3: Mechanical properties of pristine PU, PU/MGR, and PU/MGR/CuNP composites. (a) Representative stress-strain curves, (b) average failure strain, and (c) toughness of PU, PU/MGR, and PU/MGR/CuNP composites. (d) Comparison of the average failure strain of different PU composites to uncover the optimal co-reinforcement filler material.

To better understand the influence of the co-filler material in improving the failure strain of the PU/MGR composites, we also screened two other co-filler materials, namely TiO_2 and MoS_2, by introducing them into the PU/MGR composite to develop PU/MGR/TiO_2 and PU/MGR/MoS_2 composites, respectively. TiO_2 and MoS_2 were chosen because they are often used as reinforcement materials in polymer matrices [29]. However, both TiO_2 and MoS_2 led to a further decrease in the failure strain compared to PU/MGR composite (Figure 3d). Thus, the failure strain results clearly highlights the beneficial role of CuNP reinforcement in reducing

the brittle-like behavior and enhancing the ductility of the PU/MGR composite. To further visualize the magnitude of elongation in the PU composites system, we performed a unique experiment as discussed in **Supplementary Note 1**.

We now elaborate on the fundamental mechanisms for these observations that arise from the introduction of CuNPs into the PU/MGR composite and propose models to elucidate the role of CuNPs in engineering the failure strain, as illustrated in Figure 4a. Pristine PU is capable of high elongation due to the unrestricted movement of the flexible PU chains and the absence of stress concentration sites inside the matrix (Figure 4). When a high concentration of MGR filler (e.g. 2 wt%) was introduced into the PU matrix, the possibility of filler agglomeration is substantial (Figure 4a-4b). The agglomerated MGR sheets form a bunch of high-modulus particulates inside a low-modulus PU matrix. Consequently, the agglomerated MGR particulates introduce a region of high stress concentration inside the PU matrix. In addition, the low adhesive strength at the PU and MGR interface may lead to the preferential separation of the PU-MGR interfaces and result in crack initiation upon stretching. Furthermore, since the MGR fillers restrict the mobility of the PU chains to reorganize and heal the cracks, the regions of high stress concentration may increase in crack density and size with higher strain, ultimately generating voids/cavities and causing the strain localization around the dense network of MGR (Figure 4a). These lead to a drop in the ductility and yielding behavior of the PU/MGR composite. The inclusion of CuNPs leads to their accumulation on the MGR sheets, thus suppressing the agglomeration of MGR sheets by disrupting the non-covalent π-π and van der Waals interactions between the MGR sheets [30] (Figure 4b), as well as any non-covalent interactions between the MGR sheets and the PU chains. With reduced MGR agglomeration, there is an overall lower stress concentration at the filler regions that greatly decreases the likelihood of crack formation and propagation at the PU-MGR interface, and ultimately reduces void/cavity formation. As a result, increased ductility and a higher failure

strain were observed in the PU/MGR/CuNP composites (e.g. sample C1). Further, the increase in the CuNP concentration is not expected to considerably alter the stress concentration and extent of void/cavity formation, which is why the failure strain values remain similar for all PU/MGR/CuNP composite samples. We also noticed that the ultimate tensile strength (UTS) decreased by introducing and increasing the concentration of CuNP in the PU/MGR composite (*see* **Supplementary Note 2**). This is attributed to the modification of the PU-MGR interface by the CuNPs which caused increased mobility of the PU chains enabling them to slide across one another more easily at lower stresses.

Unlike the PU/MGR/CuNP composite system, the PU/MGR/TiO_2 and PU/MGR/MoS_2 composite systems largely reduced the failure strain. This may be due to a combined effect of TiO_2 or MoS_2 with MGR that leads to an enhancement in the stress concentration sites. As a result, PU chain mobility is severely restricted, and hence decreased elongation and more brittle-like character is observed. The use of different co-filler materials thus reveals the importance of co-filler material selection for the PU/MGR composite system and demonstrates the advantage of CuNP in increasing the ductility of the PU/MGR composite system. Separately, we have also measured the UTS of PU/MGR/TiO_2 and PU/MGR/MoS_2 composites which revealed anomalous behavior, as discussed in **Supplementary Note 2.**

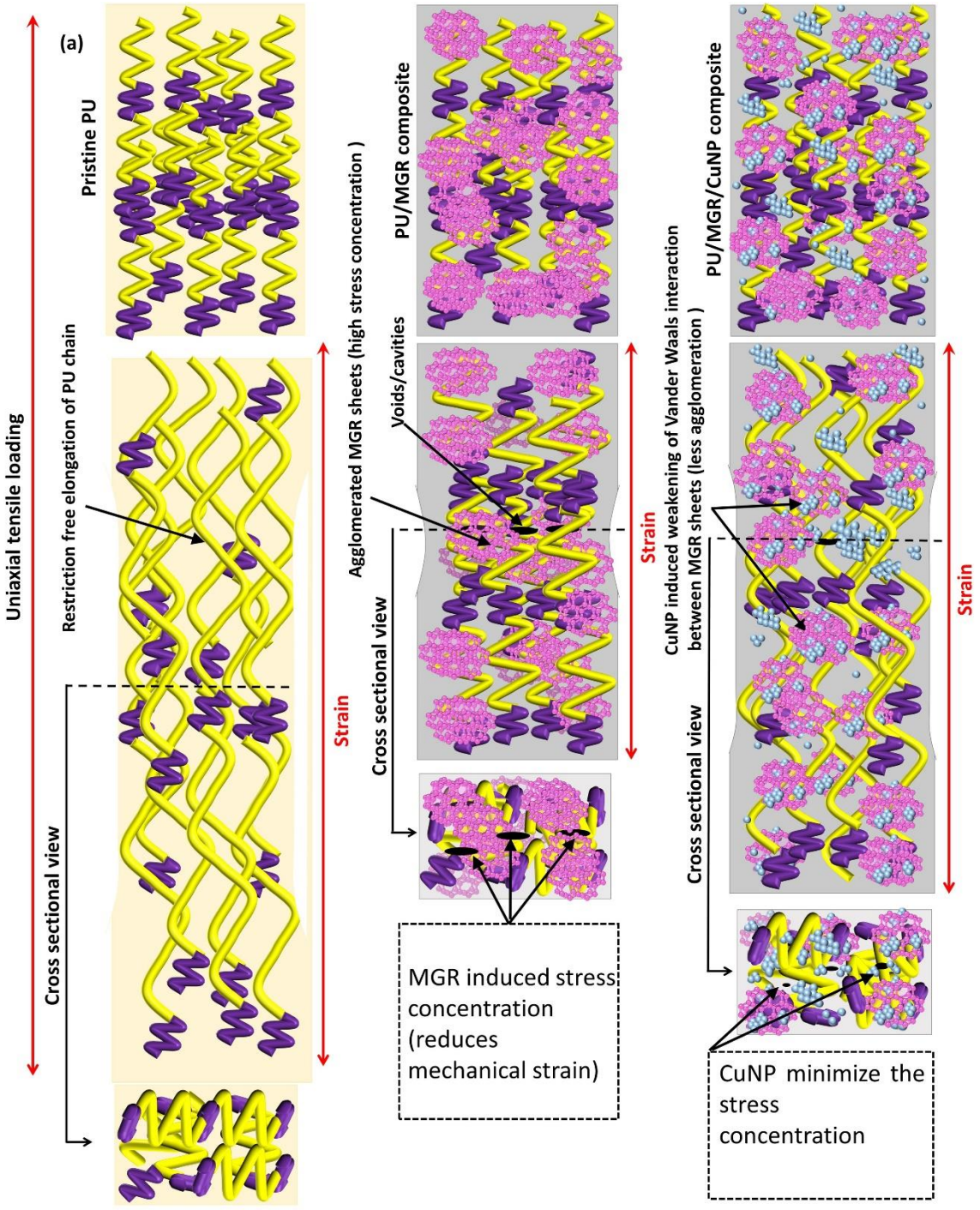
(a)
Pristine PU
Uniaxial tensile loading
Restriction free elongation of PU chain
Cross sectional view
Strain
PU/MGR composite
Agglomerated MGR sheets (high stress concentration)
Voids/cavities
Cross sectional view
Strain
MGR induced stress concentration (reduces mechanical strain)
PU/MGR/CuNP composite
CuNP induced weakening of Vander Waals interaction between MGR sheets (less agglomeration)
Cross sectional view
Strain
CuNP minimize the stress concentration

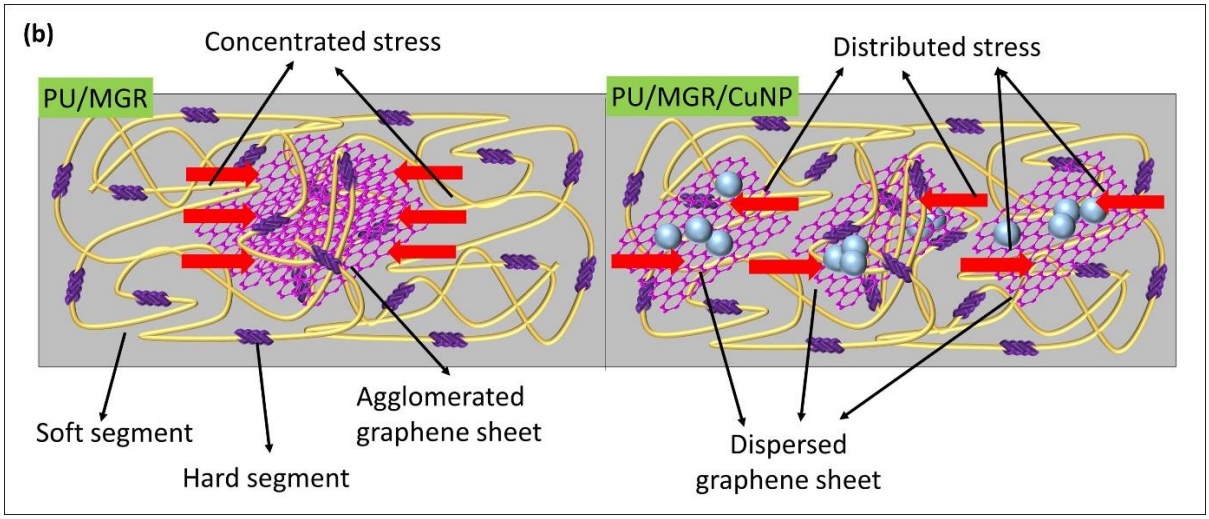

Figure 4: Schematic illustration for strain engineering mechanisms for MGR (middle) versus MGR/CuNP binary fillers (right) in the PU matrix. (b) Enlarge view of MGR accumulation in PU matrix, and hence the origin of concentrated stresses in PU/MGR composite. The introduction of CuNP reduces the MGR agglomeration by disturbing π-π and weak Vander Waals interactions between the MGR sheets, thus minimizing stress concentration to achieve large failure strain.

To obtain mechanistic insights into the MGR- and MGR/CuNP-reinforced PU systems, we extensively examined the morphologies of their respective cryo-fractured samples using FESEM (Figures 5a-5l). Pristine PU showed a smoother fracture surface and more elongated fracture (more plastic deformation before failure), suggesting its ductile-like character (Figures 5a-5b). However, the incorporation of 2 wt% MGR resulted in a rougher fracture surface in the PU/MGR composite (Figures 5c-5d). This is attributed to the void formation due to low adhesive strength at the PU-MGR interfaces. As the tensile stress/strain increases, more voids are formed until a point when the crack propagates through the voids leading to the brittle-like fracture. The roughness/morphology of the fractured surface is partially contributed by the void "pockets" that are formed just before fracture. The fracture surfaces of the PU/MGR/CuNP composites (Figure 5e-5l) appeared to be smoother than the fracture surface of the PU/MGR composite, but they were still rougher than pristine PU. Nonetheless, such a transition in the fracture surface morphology indicates the transformation of the PU/MGR composite from brittle-like failure to ductile-like failure upon CuNP co-reinforcement. EDS mapping further

confirmed the presence of CuNP on the fractured surfaces, suggesting their role in improving the elongation of the PU/MGR system (**Supplementary Note 3**).

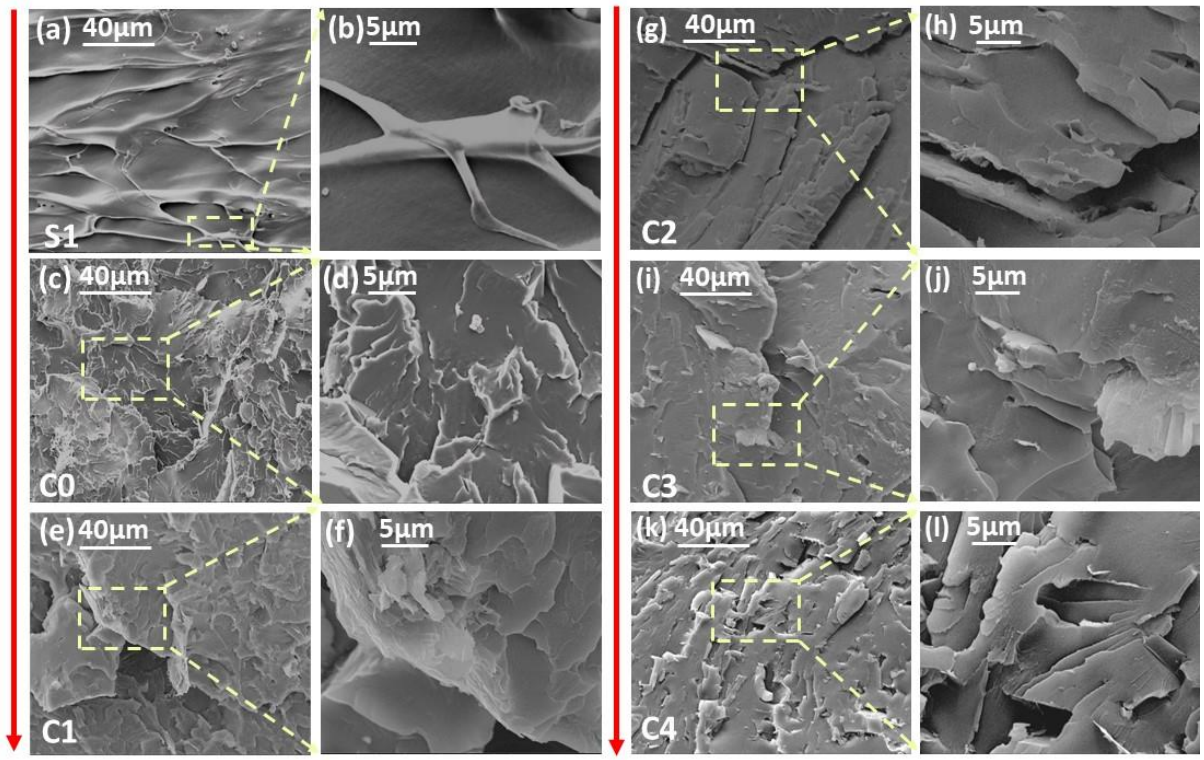

Figure 5: FESEM images of the fractured surfaces of pristine PU, PU/MGR, and PU/MGR/CuNP composites. (a-b) pristine PU, (c-d) PU/MGR composite (sample C0), (e-f) PU/MGR/CuNP at 0.1 wt% CuNP concentration (sample C1), (g-h) PU/MGR/CuNP at 0.25 wt% CuNP concentration (sample C2), (i-j) PU/MGR/CuNP at 0.5 wt% CuNP concentration (sample C3), and (k-l) PU/MGR/CuNP at 1.0 wt% CuNP concentration (sample C4).

We have so far provided strong evidence for the significant influence exerted by the co-reinforcement of CuNPs in PU/MGR composites to control its tensile properties, mainly in the modification of its strain behavior. This leads to a question of whether CuNP reinforcement also results in the modification of other mechanical properties of PU/MGR composite systems, especially their friction and wear properties which could adversely affect the performance and durability of moving mechanical systems and lead to significant energy losses as well as the need to frequently replace the systems. Therefore, we systematically investigated the sliding friction and wear properties of the PU and PU composites by sliding their surfaces against steel

balls in a ball-on-disk configuration where the sample surfaces rotate with respect to the counterface ball. The representative frictional curves, average coefficient of friction (COF) computed over the steady-state friction regime, and the optical microscope images of the counterface balls and sample wear tracks after ball-on-disk tribological tests are presented in Figures 6a-c, respectively. A schematic illustration of the tribological mechanisms and the calculated ball wear volume results are presented in Figures 6d and 6e, respectively. The tests were repeated at least 3–4 times to ensure the reproducibility of the results and they revealed the stability in the COF for the PU composite samples (***see*** **Supplementary Note 4** for details). Pristine PU demonstrated moderate level of friction that fluctuated around an average COF of ~0.37 (Figure 6a). Moreover, PU experienced considerable wear as confirmed by the large amount of debris transferred to the ball together with a very intense and wide wear track on the sample (Figure 6c). This indicated that pristine PU alone was not tribological resilient and required suitable engineering of its intrinsic material properties for tribological operations. The introduction of MGR largely improved the sliding performance of PU as confirmed by a very stable level of friction until the completion of the tests (6000 cycles) with a low average COF of ~0.11 in the PU/MGR composite (Figures 6a and 6b). Moreover, the PU/MGR composite demonstrated a large improvement in wear resistance over pristine PU, as reflected by significantly less debris transferred to the ball and a relatively fainter and narrower wear track formed on the sample (Figure 6c). This finding demonstrates why MGR type fillers are frequently used as polymer reinforcements to improve the friction and wear properties for real world applications. Interestingly, we found that the co-reinforcement of PU/MGR with CuNPs further boosted the tribological performance. All the PU/MGR/CuNP composites achieved extremely low average COFs of ~0.06, ~0.05, ~0.06 and ~0.06 in samples C1, C2, C3, and C4, respectively, approaching the regime of superlubricity, a state where friction almost vanishes (Figure 6b). Moreover, the extremely low friction could be maintained over the entire

tribological test of 6000 cycles for all the PU/MGR/CuNP composites (Figure 6a). The wear tracks of the PU/MGR/CuNP composites were much fainter and narrower than the PU/MGR composite, and the amount of debris transferred to the ball was minimal, suggesting the high wear resistance of the PU/MGR/CuNP composites. Thus, the co-reinforcement of PU/MGR with CuNP not only helped to increase the failure strain but also substantially improved the friction and wear characteristics of the PU composite which is astonishing from the scientific and technological points of view.

We now discuss the friction and wear mechanisms observed from the tribological tests. The frictional forces (F_f) strongly depend on the shear strength (τ) at the tribo-interfaces and are directly related to each other, *i.e.* a higher shear strength corresponds to higher frictional forces [31]. Thus, the COF, which varies inversely to F_f, increases with increasing τ. As discussed previously, pristine PU possesses high cohesive strength but MGR has a low shear strength. For pristine PU, which gives a PU-steel tribo-pair during the tribological tests, the high friction is mainly attributed to the relatively high shear strength of PU which resists the sliding motion of the ball at the tribo-interface. The fluctuation in COF for pristine PU can be attributed to PU deformation and stick-slip events during the tribological tests. The higher frictional forces and the softer material of pristine PU compared to the steel ball thus resulted in severe wear of the PU material caused by elastic-plastic deformation, erosion, adhesion/abrasion, and ploughing. On the other hand, the MGR reinforcement reduced the shear strength of the PU/MGR composite, compared to pristine PU, and promoted the reduction in friction due to decreased sliding resistance at the tribo-interface. The enhancement of the frictional stability in the PU/MGR composite is ascribed to reduced deformation of the bulk PU and reduced stick-slip behavior as the ball slides over more MGR fillers at the tribo-interface. Finally, we sought to uncover why CuNP co-reinforcement helped to further reduce friction and wear and attain superlubricity in the PU/MGR/CuNP composites. The mechanism responsible for the

improved sliding performance of PU due to reinforcement with the MGR/CuNP binary filler is schematically illustrated in Figure 6e. FESEM characterizations revealed the sheet-like layered morphology for MGR (Figure 2b) and the spontaneous clustering of CuNPs (Figure 2c). The combined MGR/CuNP binary filler was also characterized and showed that the CuNPs or CuNP clusters are present on MGR sheets. The presence of CuNPs on MGR surfaces serves to limit the agglomeration of MGR sheets, and in one way reduced the stress concentration around the MGR fillers as reflected by the increase in the failure strain value for MGR/CuNP reinforced PU. At the same time, these CuNPs, when decorated on MGR sheets, may be wrapped inside the flexible MGR sheets during sample preparation or tribo-sliding, and may activate nano-/micro-scale rolling events along with sliding [32]. Thus, the binary MGR/CuNP filler combination can enable even more slippery contact compared to just using MGR fillers alone. Moreover, at relatively higher concentrations (2 wt%), the MGR sheets are expected to shield the CuNP and CuNP clusters from tribo-mechanical damage and their removal from the wear track, thereby maintaining an ultralow and stable friction in the PU/MGR/CuNP composites until the completion of the tests. Additionally, as discussed previously, CuNPs can modify the PU-MGR interface such that it promotes the ease of sliding the PU chains across one another at lower shear stresses or energy, thus contributing to the reduced friction. Overall, the reduction of wear in the PU/MGR and PU/MGR/CuNP composites compared to pristine PU is mainly attributed to the reduced deformation and the reduced number of adhesive/abrasive events (typically caused by stick-slip behavior) at the sliding tribo-interfaces.

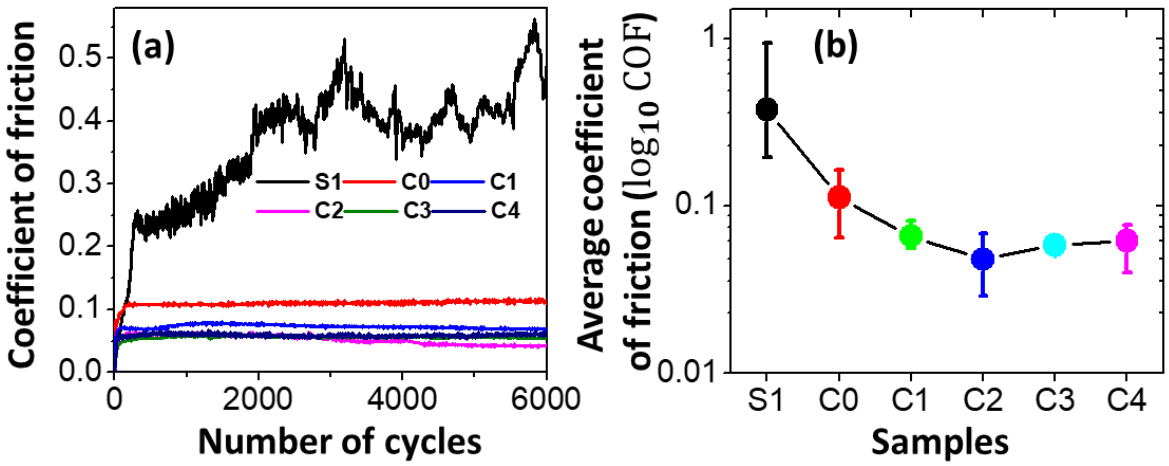
(a)
Coefficient of friction
0.0
0.1
0.2
0.3
0.4
0.5
0
2000
4000
6000
Number of cycles
S1
C0
C1
C2
C3
C4
(b)
Average coefficient of friction ($\log_{10}$ COF)
1
0.1
0.01
S1
C0
C1
C2
C3
C4
Samples

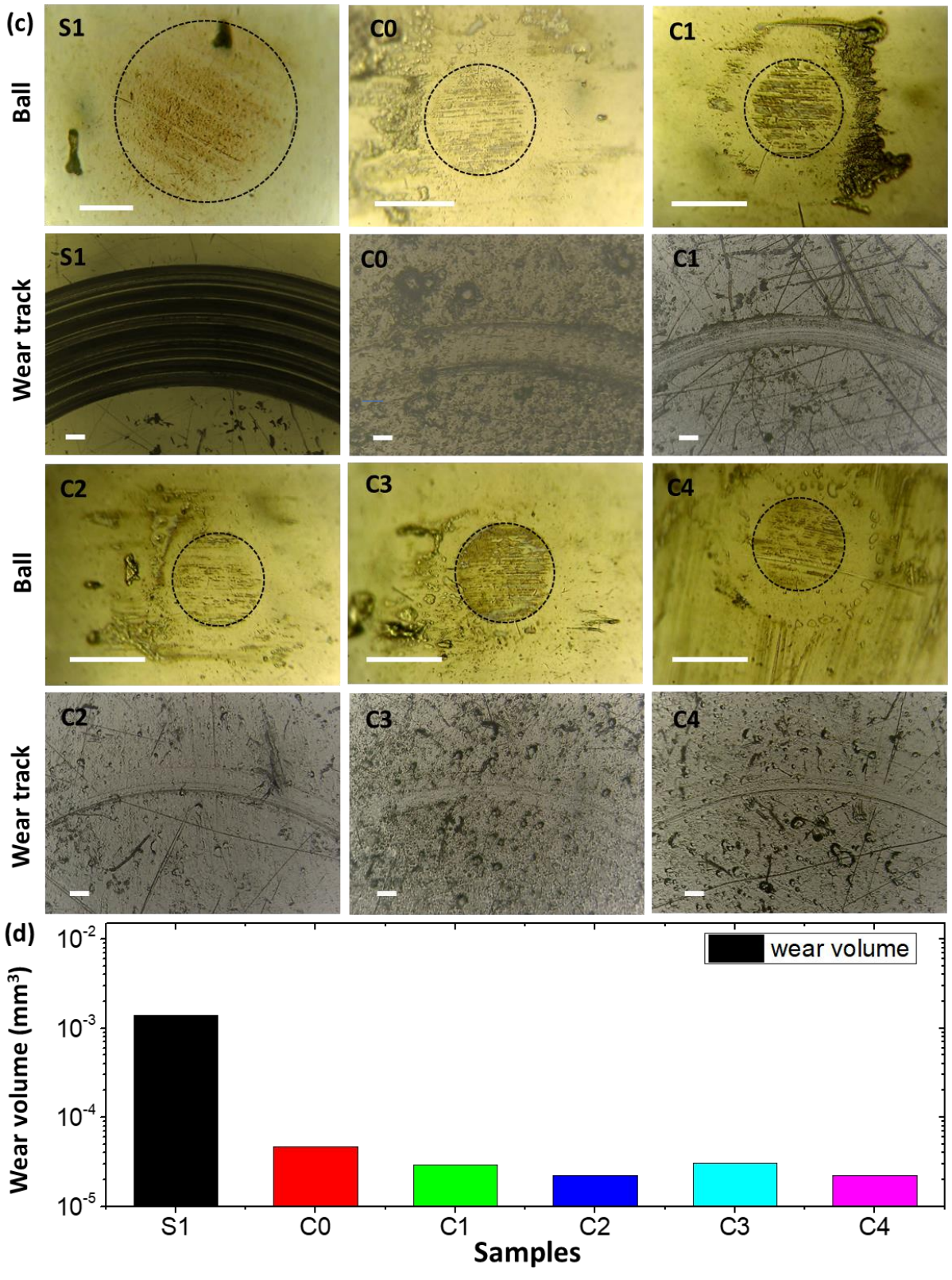
(c)
Ball
Wear track
Ball
Wear track
S1
C0
C1
S1
C0
C1
C2
C3
C4
C2
C3
C4
(d)
Wear volume (mm³)
10⁻²
10⁻³
10⁻⁴
10⁻⁵
wear volume
S1
C0
C1
C2
C3
C4
Samples

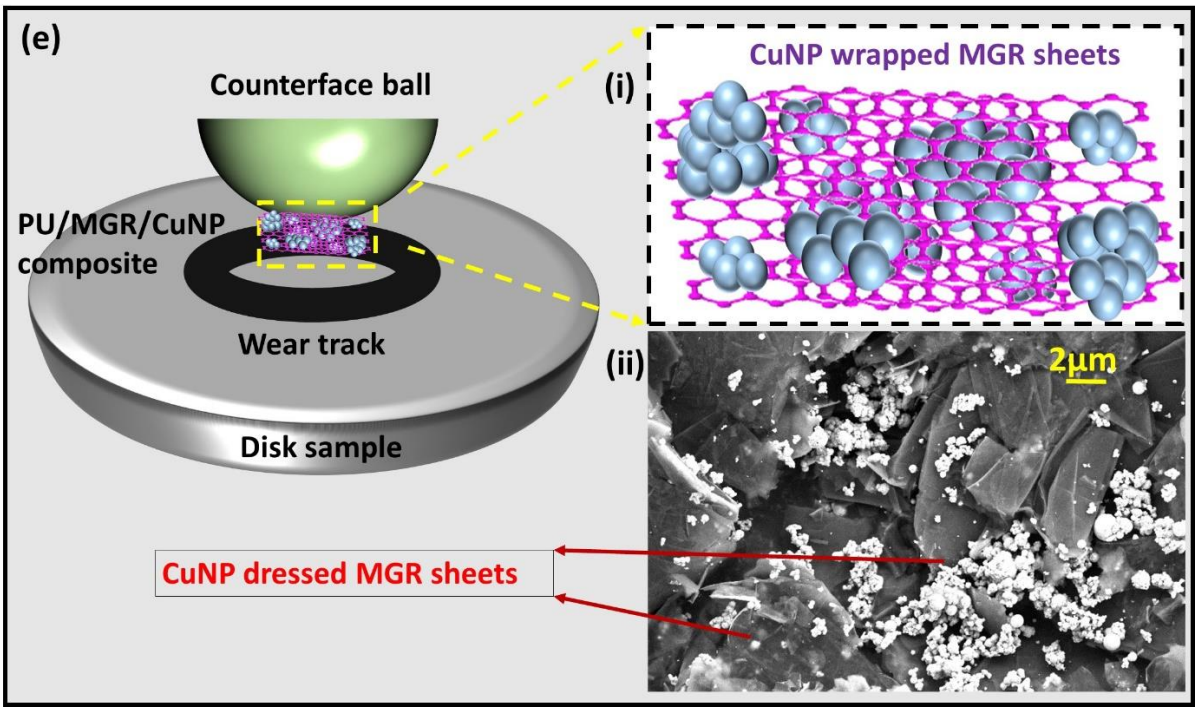

Figure 6: (a) Coefficient of friction versus number of cycles of the tribological tests, (b) average coefficient of friction computed over the steady state friction regime, (c) optical microscope images of the counterface balls and sample wear tracks for pristine PU, PU/MGR, and PU/MGR/CuNP composites. Scale bars in the optical microscope images represent 100 µm. (d) Calculated ball wear volumes for PU, PU/MGR, and PU/MGR/CuNP composite samples after the tribological tests. (e) Schematic illustration of the tribo-interface of a steel ball sliding on a PU/MGR/CuNP composite showing the presence of the MGR/CuNP binary filler material at the tribo-interface after surface wear from the initial sliding cycles; inset (i) shows a scheme illustrating the decoration of the MGR with agglomerated CuNPs which are present the tribo-interface, and inset (ii) is an actual FESEM image of the CuNP-dressed MGR sheets used in the present work.

We have also calculated the ball wear volume (Figure 6d) using Equations 5 and 6. [33]

$$V = \frac{\pi h}{6}\left(\frac{3d^2}{4} + h^2\right) \quad (5)$$

$$h = R - \sqrt{R^2 - \frac{d^2}{4}} \quad (6)$$

where V is the wear volume (mm^3), d is the diameter of the wear scar (mm), h is the depth of the wear track (mm), and R is the radius of the counterface steel ball (mm). The application of MGR reduced the ball wear volume which was even further decreased by introducing the

MGR/CuNP binary fillers. Thus, these results evidently show that CuNP-decorated MGR sheets significantly minimize the wear and deliver greater wear resistance in PU composites.

For thermo-responsive SMPs, their thermal conductivity (TC) is a key parameter that affects their performance in targeted applications. Most polymers including PU exhibit poor TC which restricts their application in thermally-triggered systems. Thus, it is of paramount interest to uncover the role of MGR and the co-reinforcement material of CuNP on the TC of PU. We have measured the TCs of the samples at three different temperatures (25 ºC, 50 ºC, and 75 ºC) (Figure 7a), and subsequently computed the TC enhancement (TCE) (in %) with respect to pristine PU (Figure 7b) using Equation 7:

$$\mathrm{TCE} = \frac{\mathrm{TC_m} - \mathrm{TC_0}}{\mathrm{TC_0}} \quad (7)$$

where TC_0 is the thermal conductivity of pristine PU and TC_m is the thermal conductivity of PU reinforced with MGR or MGR/CuNP fillers. From Figure 7a, it can be seen that the introduction of MGR and MGR/CuNP fillers boosts the TC of PU at all tested temperatures. Closer examination suggested that the extent of TC enhancement of PU is higher for the MGR /CuNP fillers than for MGR-only fillers, suggesting the promising role of CuNP co-reinforcement in improving the material's TC (Figure 7a). The TCEs at 50 ºC for samples C0, C1, C2, C3, and C4 were calculated to be 25.9%, 51.4%, 52.6%, 49.7%, and 49.7%, respectively (Figure 7b) (thermal diffusivity and specific heat results are presented in **Supplementary Note 5)**. The low TC in pristine PU is caused by the randomly oriented molecular chains of PU segments that scattering the photons. Due to the higher thermal conductivity of graphene materials [34], the introduction of MGR sheets provides thermally conductive sites within the PU matrix, which improves the heat transfer within the PU matrix and thus increases the TC. The dispersion of MGR fillers in the matrix may also help to align the PU chains and reduce photon scattering, contributing to improved TC of the PU/MGR

composite. The TC was found to be further improved by the co-reinforcement of CuNP. CuNPs, being metallic, have an inherently high TC that exceeds MGR. In the binary MGR/CuNP filler, we have seen that the CuNPs and their clusters are decorated on/across the MGR sheets. This not only provides additional highly thermally conductive sites, but also improves the dispersion of the MGR sheets, resulting in a longer thermal conduction pathway within the thermally insulating PU matrix. Collectively, this contributes to better heat transfer and an observed increase in the TC of the PU/MGR/CuNP composites.

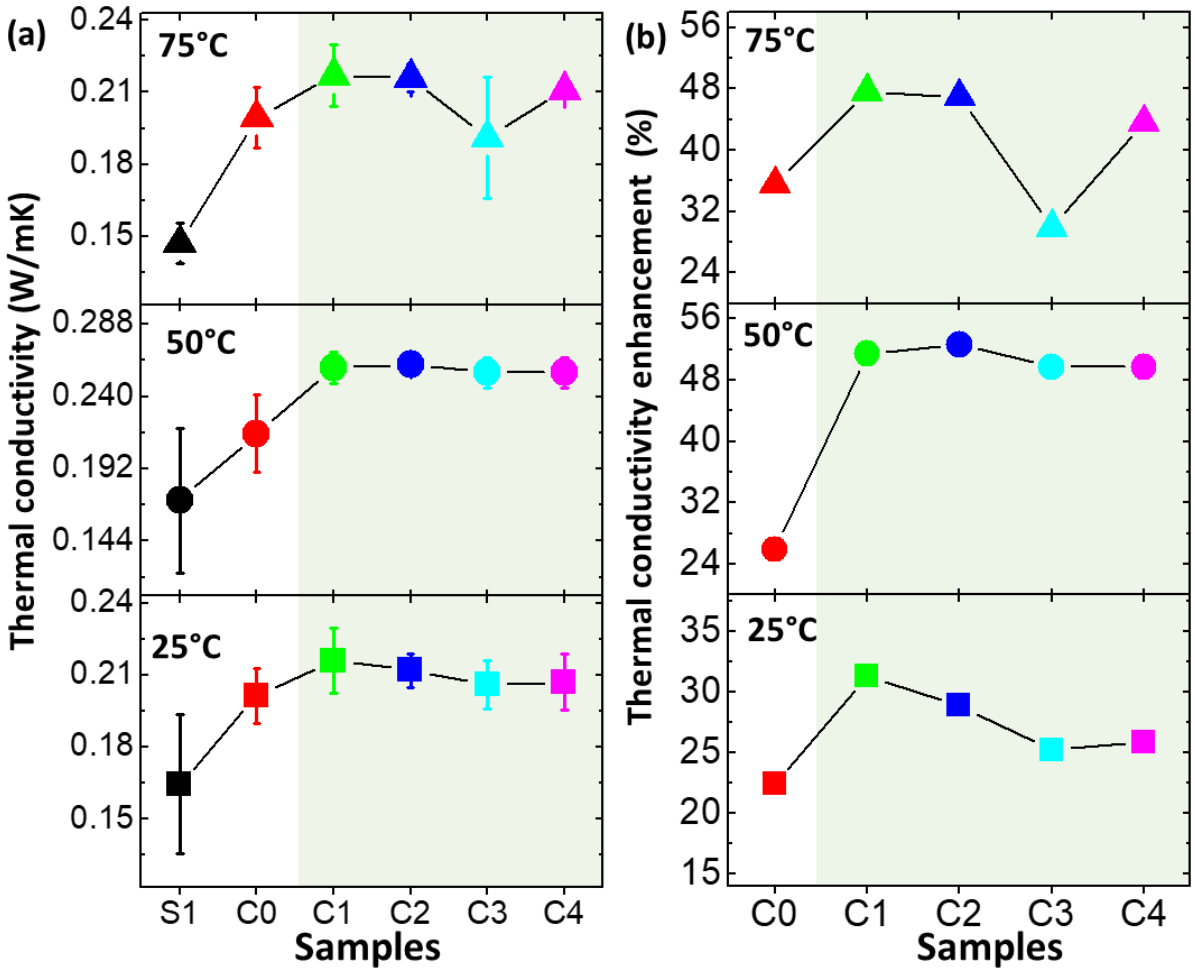

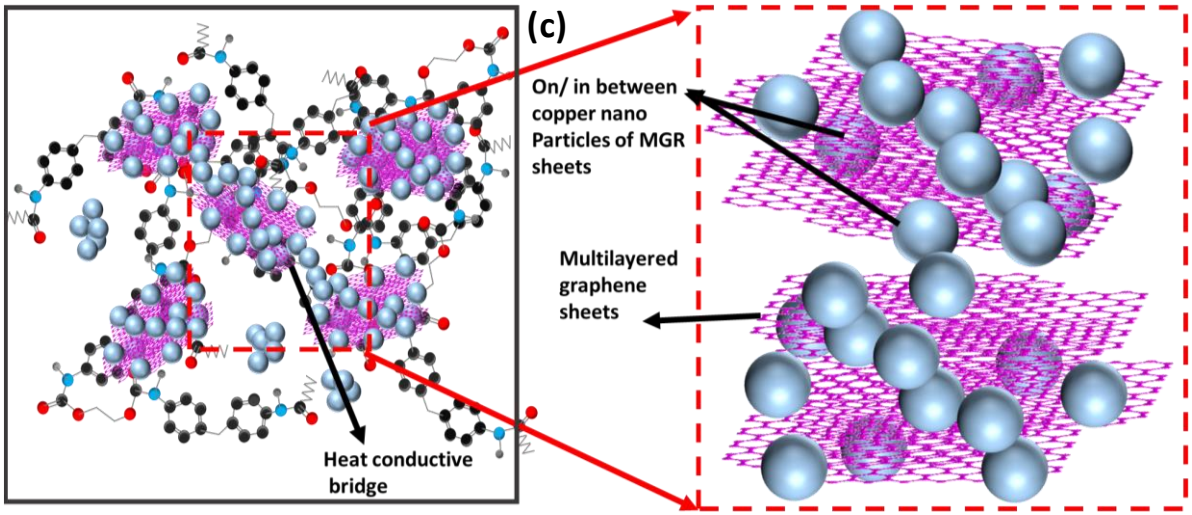

Figure 7: (a) Thermal conductivities of PU, PU/MGR, and PU/MGR/CuNP composites. (b) Thermal conductivity enhancement in PU/MGR and PU/MGR/CuNP composites with respect to pristine PU. (c) Schematic illustration of the thermal conductivity engineering mechanism by the MGR/CuNP binary fillers in the PU matrix.

Finally, we examined the shape memory behavior of the samples and whether the incorporation of CuNP had a constructive or destructive effect on the actuation of these SMPs. We mainly focused on examining the speed of actuation for the samples to attain complete shape recovery. For this purpose, the shape recovery tests were performed in a hot water (75 ºC) environment (Figure 8a). In these tests, the specimens were deformed to an angle of 30° and they had to straighten themselves to an angle of 180° to achieve complete shape recovery (see photographs in Figure 8). To determine the speed of actuation, we measured the average shape recovery time (Figure 8b), i.e. the time required for the specimen to return to its original shape from the temporary deformed shape, and from this measurement the shape recovery rate (recovered angle/time) could be determined (Figure 8c). It is evident from Figures 8a-8b that pristine PU takes about ~47 s to recover back to its original shape (*i.e.* transition from a 30° to 180° angle). The introduction of MGR fillers caused a faster shape recovery in the PU/MGR composite compared to pristine PU, with a total time of ~31 s required to achieve complete shape recovery. Interestingly, the average recovery time was further reduced to ~20 s, ~21 s, ~18.5 s, and ~31 s in samples C1, C2, C3, and C4, respectively, suggesting that faster actuation

was achieved in the PU/MGR/CuNP composites with the co-reinforcement of CuNPs. The shape recovery of these composite samples is also presented in **Supplementary Movie-2** (SM-2). It is probably not surprising that the trend of actuation/shape recovery speed follows the thermal conductivity results closely. Improved thermal conductivity in the PU/MGR/CuNP composites accounts for faster heat transport across the sample that triggers and mobilizes the soft segment chains of PU in a shorter time. Furthermore, we have also comprehensively examined the shape memory behavior of samples under repeated thermo-mechanical testing conditions (*see* **Supplementary Note 6**)**.** Briefly, the incorporation of the CuNPs enhances the shape fixity as confirmed by comparing the PU/MGR/CuNP composite sample with PU/MGR composite sample (*see* **Supplementary Note 6**).

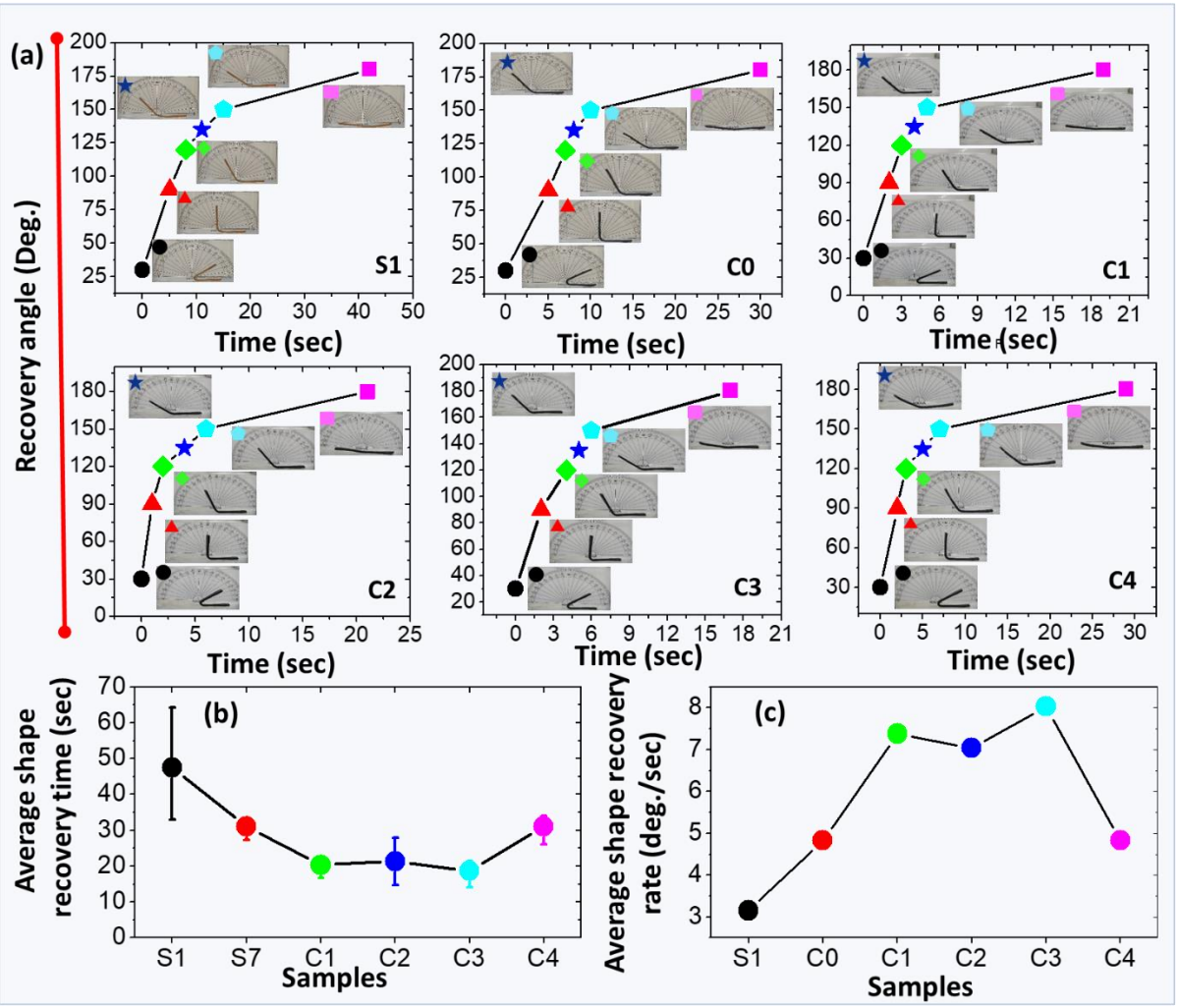

Figure 8: Shape recovery behavior of pristine PU, PU/MGR, and PU/MGR/CuNP composites in hot water (75 ℃) environment. (a) Shape recovery of the samples with time; the images in the insets represent the extent of shape recovery at certain point of time. (b) Average shape recovery time and (c) average shape recovery rate for different samples. The average shape recovery time was determined based on at least 3 measurements. The average shape recovery rate was calculated by dividing the extent of actuation (from 30° angle to 180° angle) by the average time taken to do so.

Conclusions

Through the co-reinforcement of a shape memory PU/MGR composite polymer (2.0 wt% MGR) with CuNPs, we have demonstrated the formation of PU/MGR/CuNP composites with remarkable mechanical, thermal and functional properties that make them desirable for many useful engineering applications. In PU/MGR composites, MGR fillers tend to agglomerate together due to π-π and van der Waal interactions, resulting in the formation of stress concentration sites around these fillers, resulting in lower ductility and elongation at break, thereby reducing their toughness. We have shown that CuNPs play a pivotal role in disrupting the interactions between the MGR sheets, which served to reduce their agglomeration, and suppress the number of stress concentration sites. This led to a > 200% improvement in the mechanical failure strain as well as a higher toughness in PU/MGR/CuNP composites. Furthermore, the incorporation of CuNPs was found to enhance the thermal conductivity by 20% as a result of the greater number of thermally conductive sites while also improving the dispersion of the MGR sheets within the PU matrix. In this way, longer thermal conduction pathways were created, facilitating superior heat transfer and faster shape recovery/actuation properties. In addition, CuNPs contributed to the enhanced tribological performance of PU/MGR/CuNP composites, approaching a state of superlubricity (ultralow and stable COF of ~0.05–0.06) with high wear resistance during sliding against a steel ball counterface. We hypothesize that the decoration of the graphene sheets with CuNPs, which were present at the tribo-interface, enabled the easy shearing and rolling of MGR sheets across each other, therefore significantly reducing the resistance to ball sliding at the tribo-interface. These unique

properties of CuNPs were not observed in other commonly used polymer composite co-filler materials such as TiO_2 or MoS_2. In conclusion, our work has elucidated the underlying mechanisms responsible for the superior mechanical, tribological and thermal conduction properties resulting from CuNP co-reinforcement. The mechanisms revealed in this work are likely to encourage further research into exploring other types of co-fillers with graphene sheets for precisely engineering the functional properties of polymer composite systems.

Acknowledgments

Authors wisht to thank Director, CSIR-AMPRI, Bhopal for his kind support. This research is supported by the Council of Scientific and Industrial Research (CSIR), India, through the project MLP 303. Jeet Vishwakarma acknowledges CSIR, India, for providing financial support through the GATE-JRF fellowship. The authors wish to thank Dr Rahul Mishra from IIT Delhi, and Dr Archana Singh, Dr. P. Asokan, Dr Gaurav Gupta, Dr. M. Shafeeq, Dr. D. P. Mondal, Mr. A. Khare, and Mr. D. Kashyap from CSIR-Advanced Materials and Processes Research Institute, Bhopal, India for their help.

Supporting statement:

Visualization of the magnitude of elongation in the PU composite systems: Mechanical properties of the PU, PU/MGR, and PU/MGR/CuNP composites: Energy-dispersive spectroscopy (EDS) or energy-dispersive X-ray analysis: Tribological results: Thermal

diffusivity and specific heat: Thermo-mechanical shape memory measurements, and the extraction of shape recovery ratio and shape fixity ratio for different samples: Description of the supplementary movies.

References

(1) Khan, M.; Tahir, M. N.; Adil, S. F.; Khan, H. U.; Siddiqui, M. R. H.; Al-Warthan, A. A.; Tremel, W. Graphene based metal and metal oxide nanocomposites: synthesis, properties and their applications. *Journal of Materials Chemistry A* **2015**, *3* (37), 18753-18808. Liu, G.; Jin, W.; Xu, N. Graphene-based membranes. *Chemical Society Reviews* **2015**, *44* (15), 5016-5030.
(2) Gosling, J. H.; Makarovsky, O.; Wang, F.; Cottam, N. D.; Greenaway, M. T.; Patanè, A.; Wildman, R. D.; Tuck, C. J.; Turyanska, L.; Fromhold, T. M. Universal mobility characteristics of graphene originating from charge scattering by ionised impurities. *Communications Physics* **2021**, *4* (1), 30. DOI: 10.1038/s42005-021-00518-2.
(3) Murata, H.; Nakajima, Y.; Saitoh, N.; Yoshizawa, N.; Suemasu, T.; Toko, K. High-Electrical-Conductivity Multilayer Graphene Formed by Layer Exchange with Controlled Thickness and Interlayer. *Scientific Reports* **2019**, *9* (1), 4068. DOI: 10.1038/s41598-019-40547-0.
(4) Dwivedi, N.; Ott, A. K.; Sasikumar, K.; Dou, C.; Yeo, R. J.; Narayanan, B.; Sassi, U.; Fazio, D. D.; Soavi, G.; Dutta, T.; Balci, O.; Shinde, S.; Zhang, J.; Katiyar, A. K.; Keatley, P. S.; Srivastava, A. K.; Sankaranarayanan, S. K. R. S.; Ferrari, A. C.; Bhatia, C. S. Graphene overcoats for ultra-high storage density magnetic media. *Nature Communications* **2021**, *12* (1), 2854. DOI: 10.1038/s41467-021-22687-y.
(5) Zhao, Z.; Bai, P.; Du, W.; Liu, B.; Pan, D.; Das, R.; Liu, C.; Guo, Z. An overview of graphene and its derivatives reinforced metal matrix composites: Preparation, properties and applications. *Carbon* **2020**, *170*, 302-326. DOI: https://doi.org/10.1016/j.carbon.2020.08.040.
(6) Huang, Y.; Wan, C. Controllable fabrication and multifunctional applications of graphene/ceramic composites. *Journal of Advanced Ceramics* **2020**, *9* (3), 271-291. DOI: 10.1007/s40145-020-0376-7.
(7) Papageorgiou, D. G.; Kinloch, I. A.; Young, R. J. Mechanical properties of graphene and graphene-based nanocomposites. *Progress in Materials Science* **2017**, *90*, 75-127. DOI: https://doi.org/10.1016/j.pmatsci.2017.07.004.
(8) Barani, Z.; Mohammadzadeh, A.; Geremew, A.; Huang, C.-Y.; Coleman, D.; Mangolini, L.; Kargar, F.; Balandin, A. A. Thermal Properties of the Binary-Filler Hybrid Composites with Graphene and Copper Nanoparticles. *Advanced Functional Materials* **2020**, *30* (8), 1904008. DOI: https://doi.org/10.1002/adfm.201904008 (acccessed 2023/07/18).
(9) Kim, J. T.; Jeong, H. J.; Park, H. C.; Jeong, H. M.; Bae, S. Y.; Kim, B. K. Electroactive shape memory performance of polyurethane/graphene nanocomposites. *Reactive and Functional Polymers* **2015**, *88*, 1-7. DOI: https://doi.org/10.1016/j.reactfunctpolym.2015.01.004.
(10) Ahmad, S. R.; Xue, C.; Young, R. J. The mechanisms of reinforcement of polypropylene by graphene nanoplatelets. *Materials Science and Engineering: B* **2017**, *216*, 2-9. DOI: https://doi.org/10.1016/j.mseb.2016.10.003. Yang, L.; Phua, S. L.; Toh, C. L.; Zhang, L.; Ling, H.; Chang, M.; Zhou, D.; Dong, Y.; Lu, X. Polydopamine-coated graphene as multifunctional nanofillers in polyurethane. *RSC Advances* **2013**, *3* (18), 6377-6385, 10.1039/C3RA23307C. DOI: 10.1039/C3RA23307C. Shen, M.-Y.; Chang, T.-Y.; Hsieh, T.-H.; Li, Y.-L.; Chiang, C.-L.; Yang, H.; Yip, M.-C. Mechanical Properties and Tensile Fatigue of Graphene Nanoplatelets Reinforced Polymer Nanocomposites. *Journal of Nanomaterials* **2013**, *2013*, 565401. DOI: 10.1155/2013/565401.
(11) Oh, S. M.; Oh, K. M.; Dao, T. D.; Lee, H.-i.; Jeong, H. M.; Kim, B. K. The modification of graphene with alcohols and its use in shape memory polyurethane composites. *Polymer International* **2013**, *62* (1), 54-63. DOI: https://doi.org/10.1002/pi.4366. Kausar, A.; Ur Rahman, A. Effect of graphene nanoplatelet addition on properties of thermo-responsive shape memory polyurethane-based nanocomposite. *Fullerenes, Nanotubes and Carbon Nanostructures* **2016**, *24* (4), 235-242. DOI: 10.1080/1536383X.2016.1144592. Kausar, A. Shape memory polymer/graphene nanocomposites: State-of-the-art. **2022**, *22* (1), 165-181. DOI: doi:10.1515/epoly-2022-0024 (acccessed 2023-07-19).
(12) Hager, M. D.; Bode, S.; Weber, C.; Schubert, U. S. Shape memory polymers: Past, present and future developments. *Progress in Polymer Science* **2015**, *49-50*, 3-33. DOI: https://doi.org/10.1016/j.progpolymsci.2015.04.002. Hu, J.; Zhu, Y.; Huang, H.; Lu, J. Recent

advances in shape–memory polymers: Structure, mechanism, functionality, modeling and applications. *Progress in Polymer Science* **2012**, *37* (12), 1720-1763. DOI: https://doi.org/10.1016/j.progpolymsci.2012.06.001. Zhang, Y.; Hu, J. Isocyanate Modified GO Shape-Memory Polyurethane Composite. In *Polymers*, 2020; Vol. 12.
(13) Jung, Y. C.; Kim, J. H.; Hayashi, T.; Kim, Y. A.; Endo, M.; Terrones, M.; Dresselhaus, M. S. Fabrication of Transparent, Tough, and Conductive Shape-Memory Polyurethane Films by Incorporating a Small Amount of High-Quality Graphene. *Macromolecular Rapid Communications* **2012**, *33* (8), 628-634. DOI: https://doi.org/10.1002/marc.201100674 (acccessed 2023/07/19).
(14) Lotfi Mayan Sofla, R.; Rezaei, M.; Babaie, A.; Nasiri, M. Preparation of electroactive shape memory polyurethane/graphene nanocomposites and investigation of relationship between rheology, morphology and electrical properties. *Composites Part B: Engineering* **2019**, *175*, 107090. DOI: https://doi.org/10.1016/j.compositesb.2019.107090.
(15) Abbasi, A.; Mir Mohamad Sadeghi, G.; Ghasemi, I.; Shahrousvand, M. Shape memory performance of green in situ polymerized nanocomposites based on polyurethane/graphene nanoplatelets: Synthesis, properties, and cell behavior. *Polymer Composites* **2018**, *39* (11), 4020-4033. DOI: https://doi.org/10.1002/pc.24456.
(16) Shi, H.-H.; Ruan, H.-X.; Chen, Z.-J.; Zhang, Y.; Zou, C.-L.; Zhang, X.-C.; Liu, B.; Xu, M.-J.; Li, B. Shape memory, thermal conductivity, and mechanical property of polylactic acid and natural rubber composites reinforced by an inorganic thermal conductive network. *Journal of Applied Polymer Science* **2022**, *139* (30), e52668. DOI: https://doi.org/10.1002/app.52668 (acccessed 2023/07/13).
(17) Jiu, H.; Jiao, H.; Zhang, L.; Zhang, S.; Zhao, Y. Graphene-crosslinked two-way reversible shape memory polyurethane nanocomposites with enhanced mechanical and electrical properties. *Journal of Materials Science: Materials in Electronics* **2016**, *27* (10), 10720-10728. DOI: 10.1007/s10854-016-5173-2.
(18) Wang, J.; Jin, X.; Wu, H.; Guo, S. Polyimide reinforced with hybrid graphene oxide @ carbon nanotube: Toward high strength, toughness, electrical conductivity. *Carbon* **2017**, *123*, 502-513. DOI: https://doi.org/10.1016/j.carbon.2017.07.055.
(19) Guan, L.-Z.; Wan, Y.-J.; Gong, L.-X.; Yan, D.; Tang, L.-C.; Wu, L.-B.; Jiang, J.-X.; Lai, G.-Q. Toward effective and tunable interphases in graphene oxide/epoxy composites by grafting different chain lengths of polyetheramine onto graphene oxide. *Journal of Materials Chemistry A* **2014**, *2* (36), 15058-15069, 10.1039/C4TA02429J. DOI: 10.1039/C4TA02429J.
(20) Panova, T. V.; Efimova, A. A.; Berkovich, A. K.; Efimov, A. V. Plasticity control of poly(vinyl alcohol)–graphene oxide nanocomposites. *RSC Advances* **2020**, *10* (40), 24027-24036, 10.1039/D0RA04150E. DOI: 10.1039/D0RA04150E.
(21) Parameswaranpillai, J.; Joseph, G.; Shinu, K. P.; Sreejesh, P. R.; Jose, S.; Salim, N. V.; Hameed, N. The role of SEBS in tailoring the interface between the polymer matrix and exfoliated graphene nanoplatelets in hybrid composites. *Materials Chemistry and Physics* **2015**, *163*, 182-189. DOI: https://doi.org/10.1016/j.matchemphys.2015.07.028.
(22) Friedrich, K. Polymer composites for tribological applications. *Advanced Industrial and Engineering Polymer Research* **2018**, *1* (1), 3-39. DOI: https://doi.org/10.1016/j.aiepr.2018.05.001.
(23) Vishwakarma, J.; Jaiswal, S.; Bharti, P.; Dhand, C.; Kumar, R.; Hashmi, S. A. R.; Srivastava, A. K.; Dwivedi, N. Competing and decisive roles of 1D/2D/3D sp2-carbons in controlling the shape switching, contact sliding, and functional properties of polymers. *Materials Today Chemistry* **2022**, *25*, 100960. DOI: https://doi.org/10.1016/j.mtchem.2022.100960.
(24) Guadagno, L.; Sarno, M.; Vietri, U.; Raimondo, M.; Cirillo, C.; Ciambelli, P. Graphene-based structural adhesive to enhance adhesion performance. *RSC Advances* **2015**, *5* (35), 27874-27886, 10.1039/C5RA00819K. DOI: 10.1039/C5RA00819K.
(25) Li, Z.; Chang, S.; Khuje, S.; Ren, S. Recent Advancement of Emerging Nano Copper-Based Printable Flexible Hybrid Electronics. *ACS Nano* **2021**, *15* (4), 6211-6232. DOI: 10.1021/acsnano.1c02209.

(26) Sarkar, J.; Chakraborty, N.; Chatterjee, A.; Bhattacharjee, A.; Dasgupta, D.; Acharya, K. Green Synthesized Copper Oxide Nanoparticles Ameliorate Defence and Antioxidant Enzymes in Lens culinaris. In *Nanomaterials*, 2020; Vol. 10.
(27) Aguiar, R.; Miller, R. E.; Petel, O. E. Microstructural evidence of the toughening mechanisms of polyurethane reinforced with halloysite nanotubes under high strain-rate tensile loading. *Scientific Reports* **2021**, *11* (1), 13161. DOI: 10.1038/s41598-021-92663-5.
(28) Liu, J. A. C.; Gillen, J. H.; Mishra, S. R.; Evans, B. A.; Tracy, J. B. Photothermally and magnetically controlled reconfiguration of polymer composites for soft robotics. *Science Advances 5* (8), eaaw2897. DOI: 10.1126/sciadv.aaw2897 (acccessed 2024/07/31). Piskarev, Y.; Sun, Y.; Righi, M.; Boehler, Q.; Chautems, C.; Fischer, C.; Nelson, B. J.; Shintake, J.; Floreano, D. Fast-Response Variable-Stiffness Magnetic Catheters for Minimally Invasive Surgery. *Advanced Science* **2024**, *11* (12), 2305537. DOI: https://doi.org/10.1002/advs.202305537 (acccessed 2024/08/01). Yadav, P. R.; Rizvi, M. H.; Kuttich, B.; Mishra, S. R.; Chapman, B. S.; Lynch, B. B.; Kraus, T.; Oldenburg, A. L.; Tracy, J. B. Plasmon-Coupled Gold Nanoparticles in Stretched Shape-Memory Polymers for Mechanical/Thermal Sensing. *ACS Applied Nano Materials* **2021**, *4* (4), 3911-3921. DOI: 10.1021/acsanm.1c00309.
(29) Wang, X.; Xing, W.; Feng, X.; Song, L.; Hu, Y. MoS2/Polymer Nanocomposites: Preparation, Properties, and Applications. *Polymer Reviews* **2017**, *57* (3), 440-466. DOI: 10.1080/15583724.2017.1309662. Cazan, C.; Enesca, A.; Andronic, L. Synergic Effect of TiO2 Filler on the Mechanical Properties of Polymer Nanocomposites. In *Polymers*, 2021; Vol. 13.
(30) Zhan, J.; Lei, Z.; Zhang, Y. Non-covalent interactions of graphene surface: Mechanisms and applications. *Chem* **2022**, *8* (4), 947-979. DOI: https://doi.org/10.1016/j.chempr.2021.12.015.
(31) Mishra, T.; de Rooij, M.; Shisode, M.; Hazrati, J.; Schipper, D. J. Characterization of interfacial shear strength and its effect on ploughing behaviour in single-asperity sliding. *Wear* **2019**, *436-437*, 203042. DOI: https://doi.org/10.1016/j.wear.2019.203042.
(32) Meng, Y.; Su, F.; Chen, Y. Synthesis of nano-Cu/graphene oxide composites by supercritical CO2-assisted deposition as a novel material for reducing friction and wear. *Chemical Engineering Journal* **2015**, *281*, 11-19. DOI: https://doi.org/10.1016/j.cej.2015.06.073.
(33) Berman, D.; Deshmukh, S. A.; Sankaranarayanan, S. K. R. S.; Erdemir, A.; Sumant, A. V. Extraordinary Macroscale Wear Resistance of One Atom Thick Graphene Layer. *Advanced Functional Materials* **2014**, *24* (42), 6640-6646. DOI: https://doi.org/10.1002/adfm.201401755.
(34) Balandin, A. A. Phononics of Graphene and Related Materials. *ACS Nano* **2020**, *14* (5), 5170-5178. DOI: 10.1021/acsnano.0c02718.

TOC

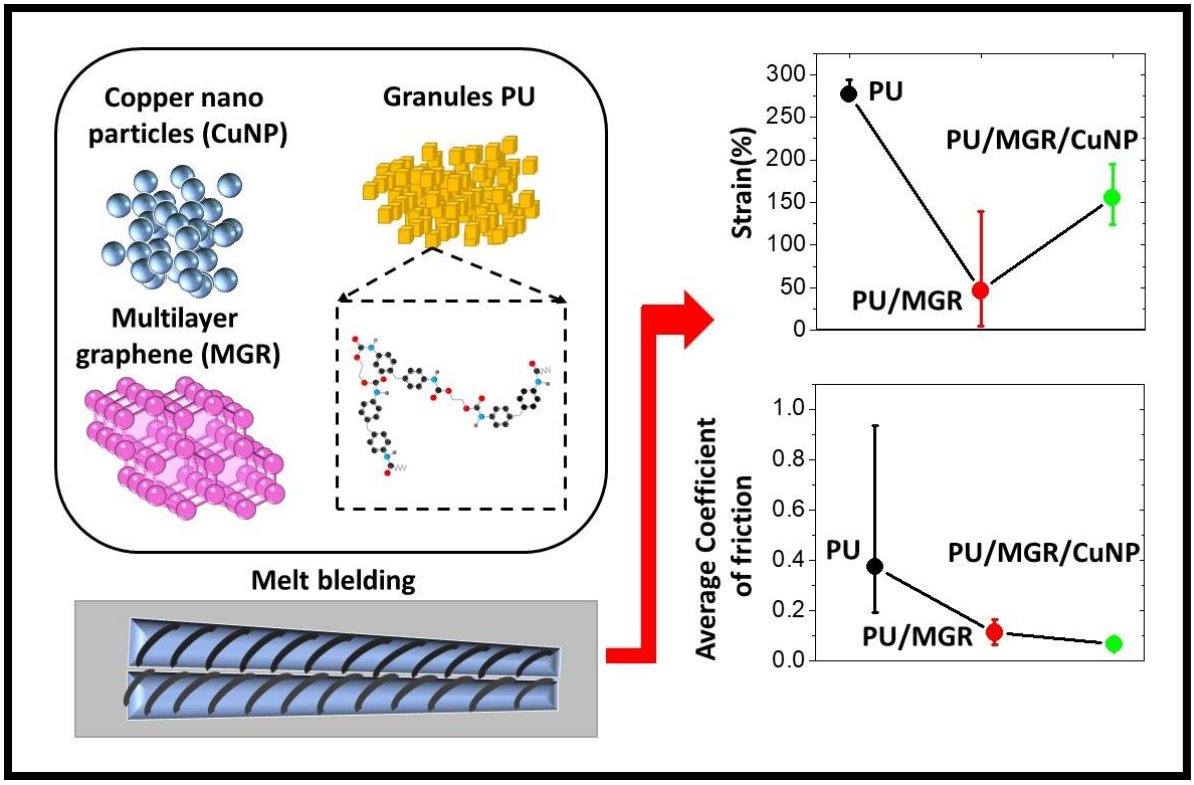
Copper nano particles (CuNP)
Granules PU
Multilayer graphene (MGR)
Melt blelding
Strain(%)
300
250
200
150
100
50
0
PU
PU/MGR/CuNP
PU/MGR
Average Coefficient of friction
1.0
0.8
0.6
0.4
0.2
0.0
PU
PU/MGR/CuNP
PU/MGR